Modes of angular motion in intrashell $^{2S+1}S^o$ states of four-valence-electron atomic systems

Bao Cheng-guang
Chinese Center of Advanced Science and Technology (World Laboratory), P. O. Box 8730, Beijing 100080, China
and Department of Physics, Zhongshan University, Guangzhou, China
(Received 16 June 1992)

A model with all the radial degrees of freedom frozen is used to simulate the intrashell states of four-valence-electron atomic systems. By inspecting the two- and three-body densities, and by inspecting directly the eigenfunctions in appropriate subspaces, the features of geometric structure and of internal motion have been obtained. The effect of the spatial permutation symmetry has been emphasized. Although the interactions are spin independent, the correlations are found to be strongly spin dependent. All odd-parity states under consideration prefer the conjugate circles (CC) structure (two circles have a common diameter and have their planes vertical to each other). Two modes of motion are found in this structure, namely, the four-body head-on collision mode and the double two-body collisions mode. It is confirmed that the modes found in the quantum states are closely related to periodic solutions of classical mechanics.

PACS number(s): 31.50.+w, 03.65.Ge, 31.20.Tz, 31.20.Di

I. INTRODUCTION

This paper is dedicated to the investigation of electron-electron (e-e) correlation of four valence-electron systems. The physics involved is expected to be much richer than that of two-electron systems. Besides, the four-valence-electron atom (e.g., carbon) is particularly important in atomic physics because it is a typical model of nonmetal elements. Hence, though the correlations would be very complicated, it is worth analyzing them.

In general, particle-particle correlations can be revealed by correlation-density functions. First, the two-body correlation can be described by two-body densities. However, the character of correlation in few-body systems is collective; the correlation between a pair of particles may be strongly affected by the disturbance of other particles. Hence, the understanding of two-body correlations alone is not sufficient. In addition, the understanding of three- and four-body correlation is also necessary. Owing to the collective correlation, the description based on independent-particle motion fails. Instead, the internal motion is of collective nature, and it appears as specific modes. In [1], a procedure for the calculation and the analysis of the one-, two-, and three-body densities was proposed, where the information from the one-body density serves as an input in analyzing the two-body density, and the information from the two-body density serves as an input in analyzing the three-body density. This procedure was found to be effective for understanding the geometric structures and internal motions of a four-body nuclear system. In [2–6], e-e correlations and the geometric behavior of intrashell states of two- and three-electron atoms have been studied by multiconfiguration Hartree-Fock (MCHF) methods; average radii and average angular separation have been calculated; in particular, two-body densities have been explicitly shown. An outcome of [5] shows that the average radii of different MCHF orbitals ($4p$, $4d$, and $4f$) are nearly the same. This finding supports the r-frozen approximation (all r_i are given at an optimal value), which was used in [7] to investigate the moleculelike rotational manifold structure of the triply excited lithium states.

Recently, the r-frozen model has also been used in [8–10] to investigate the internal collective motions in the triply excited states, where different modes of motion have been discovered. In the present paper, the same approximation and the same procedure as in [8–10] have been adopted to investigate the quadruply excited intrashell states. The main concern is also the features of internal motions. The reader is reminded that the topological structure of the nodal surfaces of the wave function determines the basic feature of the system. In realistic intrashell states, when the valence electrons move in a broad region of the main (outermost) shell, there is no nodal surface arising from radial motion (unless an electron occasionally leaves the main shell); all nodal surfaces, if there are any, are related to angular motion. Hence, the intrashell states will be characterized by their angular motion and not by their radial motion. For this reason, the r-frozen model is acceptable in the qualitative sense. Furthermore, the degrees of freedom of inner electrons, if there are any, are also considered as frozen. In general this assumption is poor. However, if the inner shells are filled up, there is no room for the inner electrons to alter their status (e.g., the two $1s$ electrons have to couple to $L=0$ and $S=0$), unless one of the valence electrons occasionally comes in. In this case, this assumption is also acceptable in the qualitative sense.

The idea of spin-dependent correlation density defined in [8] has been introduced in this paper and has been generalized to three-body density. This idea turns out to be essential. Although the e-e interaction is spin independent, the e-e correlation is found, as shown in [8] and as we shall see, to be strongly spin dependent. Hence a spin-dependent analysis is indispensable.

The idea of successive analysis of the one-, two-, and three-body densities of [1] and [8] has been introduced in this paper. It is recalled that the wave function is far from uniform but usually distributed mostly in a small region of the phase space due to correlation. The above-mentioned way of analysis can direct us to select an appropriate subspace to expose the main feature of the wave function.

In [8–10] the effect of quantum-mechanical symmetry on the structure and motion is particularly emphasized. It turns out that this symmetry is a decisive factor in microscopic structure, as shown in [8–10] and as shown below. Hence, the effect of symmetry is also emphasized in this paper. In what follows the details of the procedure and the results will be presented; only the lowest intrashell states of $^{2S+1}S^o$ symmetry ($S=2$, 1, or 0) are reported here.

II. PROCEDURE

In the r-frozen model, the Hamiltonian is

$$H=\frac{\hbar^2}{2mr_0^2}\sum_{i=1}^{4}\hat{\ell}_i^2+\sum_{i<j}\frac{e^2}{|\mathbf{r}_i-\mathbf{r}_j|}\ , \tag{1}$$

where m is the mass of the electron, l_i is the orbital angular momentum of the ith electron e_i relative to the nucleus, and $\hat{\ell}_i$ is its operator, $\mathbf{r}_i=r_0\hat{\mathbf{r}}_i$, and r_0 is the radius of the sphere not sensitive to our qualitative results. In this paper r_0 is given as 0.62 Å [11] to simulate the carbon atom. The effect of r_0 will be evaluated in Sec. VI.

The Hamiltonian is diagonalized in a model space spanned by basis functions

$$\tilde{\Phi}_i=\mathcal{A}\{[(Y_{l_1}(\hat{1})Y_{l_2}(\hat{2}))_{l_{12}}(Y_{l_3}(\hat{3})Y_{l_4}(\hat{4}))_{l_{34}}]_L \times\chi^{M_S}_{s_1s_2S}(1234)\} \tag{2}$$

where $\mathcal{A}$ is the antisymmetrizer; $\chi^{M_S}_{s_1s_2S}(1234)$ is the spin part, where the spins of particles 1 and 2 are coupled to s_1 and those of 3 and 4 are coupled to s_2; s_1 and s_2 are coupled to the total spin S, M_S is the Z component of S. In our case, $L=0$, $l_1+l_2+l_3+l_4=$odd, $S=2$, 1, or 0. l_i is restricted such that $l_i\le l_{\max}=2$ (although the electrons are supposed to stay in the $N=2$ shell, l_i of intrashell states may be higher than those allowed by the independent electron model). The effect of altering $l_{\max}$ will be also evaluated in Sec. VI, where we find that the effect is small if only the lowest states of each $^{2S+1}S^o$ symmetry are concerned.

After the diagonalization, we obtained the energy spectrum shown in Fig. 1. Among the three types of symmetry, the lowest state of the $^5S^o$ symmetry has the lowest energy, 160.56 eV (it is considered as the zero point of the spectrum). Besides, this lowest state has an extraordinarily large energy gap with its first excited state. Thus the stability of the lowest $^5S^o$ state is remarkable.

The eigenfunctions are expanded as

$$\Psi_i=\sum_j\zeta_{ij}\tilde{\Phi}_j\ . \tag{3}$$

They will be analyzed in detail. Since the spatial correlation is strongly affected by the spins, the antisymmetrized Ψ_i is further expanded as

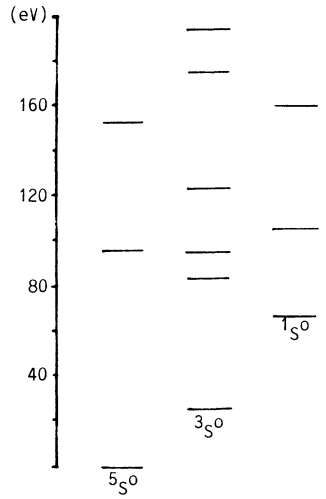

FIG. 1. Energy spectrum of the $^5S^o$, $^3S^o$, and $^1S^o$ states relative to the lowest $^5S^o$ state. This lowest state has energy 160.56 eV, which includes the kinetic energy of angular motion and e-e repulsion.

$$\Psi_i=\sum_{\mu_1,\mu_2,\mu_3}f_{\mu_1\mu_2\mu_3}(\hat{1},\hat{2},\hat{3},\hat{4})\xi_{\mu_1}(1)\xi_{\mu_2}(2)\xi_{\mu_3}(3)\xi_{\mu_4}(4)\ , \tag{4}$$

where $\xi_{\mu_i}(i)$ is the spin state of e_i, $\mu_i=\frac{1}{2}$ or $-\frac{1}{2}$, $\mu_4=M_S-\mu_1-\mu_2-\mu_3$.

From Eq. (4) we define the spin-dependent two-body density as

$$\rho_{\mu_1\mu_2}(\mathcal{R}\theta_{12})=\frac{8\pi^2}{2L+1}\sum_{\mu_3}\int d\hat{\mathbf{r}}_3 d\hat{\mathbf{r}}_4\left|f_{\mu_1,\mu_2,\mu_3}\right|^2\ , \tag{5}$$

where $\mathcal{R}$ labels the orientation of a body frame fixed at the plane formed by $\hat{\mathbf{r}}_1$ and $\hat{\mathbf{r}}_2$ (the details of how to fix it are irrelevant), and θ_{12} is the angle between $\hat{\mathbf{r}}_1$ and $\hat{\mathbf{r}}_2$. Furthermore, the weighted spin-dependent two-body density is defined as

$$\tilde{\rho}_{\mu_1\mu_2}=(\sin\theta_{12})\rho_{\mu_1\mu_2}\ . \tag{6}$$

In our case ($L=0$), $f_{\mu_1\mu_2\mu_3}$ is isotropic; thus we have

$$1=\sum_{\mu_1\mu_2}\int d\theta_{12}\tilde{\rho}_{\mu_1\mu_2}\ . \tag{7}$$

Equation (7) tells us that $\tilde{\rho}_{\frac{1}{2}\frac{1}{2}}$ is the probability density of the two electrons under observation having angular separation θ_{12} and having their spins both up, $\tilde{\rho}_{\frac{1}{2}\frac{1}{2}}+\tilde{\rho}_{\bar{\frac{1}{2}}\bar{\frac{1}{2}}}=2\tilde{\rho}_{\frac{1}{2}\frac{1}{2}}$ is the corresponding density but having one up and one down, and so on. The spin-dependent density is related to the usual two-body density by

$$\rho_2=\sum_{\mu_1,\mu_2}\rho_{\mu_1\mu_2}\ \text{ and }\ \tilde{\rho}_2=\sum_{\mu_1,\mu_2}\tilde{\rho}_{\mu_1,\mu_2}\ . \tag{8}$$

Similarly, we can define the spin-dependent three-body density as

$$\rho_{\mu_1\mu_2\mu_3} = \int d\hat{\mathbf{r}}_4 |f_{\mu_1\mu_2\mu_3}|^2 , \tag{9}$$

fulfilling

$$1 = \sum_{\mu_1,\mu_2,\mu_3} \int d\hat{\mathbf{r}}_1 d\hat{\mathbf{r}}_2 d\hat{\mathbf{r}}_3 \rho_{\mu_1\mu_2\mu_3} . \tag{10}$$

These densities have analytical expression; thus they are conveniently calculated numerically. The derivation of the analytical expressions is referred to the Appendix. In what follows, two- and three-body densities will first be analyzed to direct us into an appropriate subspace; then the wave function will be directly inspected.

III. LOWEST $^5S^o$ STATE

This state has all-antisymmetric spatial permutation symmetry. For the convenience of analysis, M_S is given as 2. It implies that all electrons have their spins up. The choice of M_S is irrelevant here.

The (weighted) spin-dependent two-body densities are shown in Figs. 2(a) and 2(a'), respectively. There is a peak at $\theta_{12}=103°=\bar{\theta}_{\uparrow\uparrow}$ in 2(a'), where $\bar{\theta}_{\uparrow\uparrow}$ labels the most probable angular separation of a pair of spin-parallel electrons. If the electrons formed a shape other than the equilateral tetrahedron (ETH), there might be more than one peak in $\tilde{\rho}_2=\tilde{\rho}_{\frac{1}{2}\frac{1}{2}}$. Hence, Figs. 2(a) and 2(a') suggest that the most probable shape may be close to an ETH.

Let $\phi_1=\phi_2=0°$, $\theta_1=90°-\bar{\theta}_{\uparrow\uparrow}/2$, and $\theta_2=90°+\bar{\theta}_{\uparrow\uparrow}/2$ (such that θ_{12} is given at $\bar{\theta}_{\uparrow\uparrow}$), then $\rho_{\frac{1}{2}\frac{1}{2}\frac{1}{2}}$ as a function of $\hat{\mathbf{r}}_3$ is plotted in Fig. 3(a). There are two features:

(i) There is a peak at ($\theta=90°$, $\phi=132°$) shown in the figure; evidently ($\theta=90°$, $\phi=-132°$) is also associated with a peak, but is not shown in the figure. e_3 and e_4 might both stay inside one of the two peaks or stay separately in two peaks. However, from Fig. 2(a) we know that two electrons are not likely to be close to each other; hence the first possibility can be ignored. The second possibility implies that e_3 and e_4 are situated in the X-Y plane symmetric with respect to the X-axis, and thus the most probable shape is an ETH as suggested. Since the ETH is the best choice to reduce the e-e repulsion, this explains why the energy of this state is the lowest.

(ii) If we ignore e_3 but observe e_4, then the distribution is the same simply because the wave function is antisymmetrized. In other words, both e_3 and e_4 prefer to have $\theta_3=\theta_4=90°$ and $\phi_3=-\phi_4$. Let us replot Fig. 3(a) with a bigger or smaller θ_{12}. We find the feature of distribution stays the same. Let us define a pair of circles of the same size having a common diameter and having their planes perpendicular to each other (e.g., the X-Z plane and X-Y plane) as conjugate circles (CC) and the common diameter (the X-axis) the intersection axis. The above findings show that the four electrons are in two pairs, and each pair stays in one of the circles symmetric to the intersection axis. We call this a CC structure. It turns out that the CC structure plays an important role in odd-parity states.

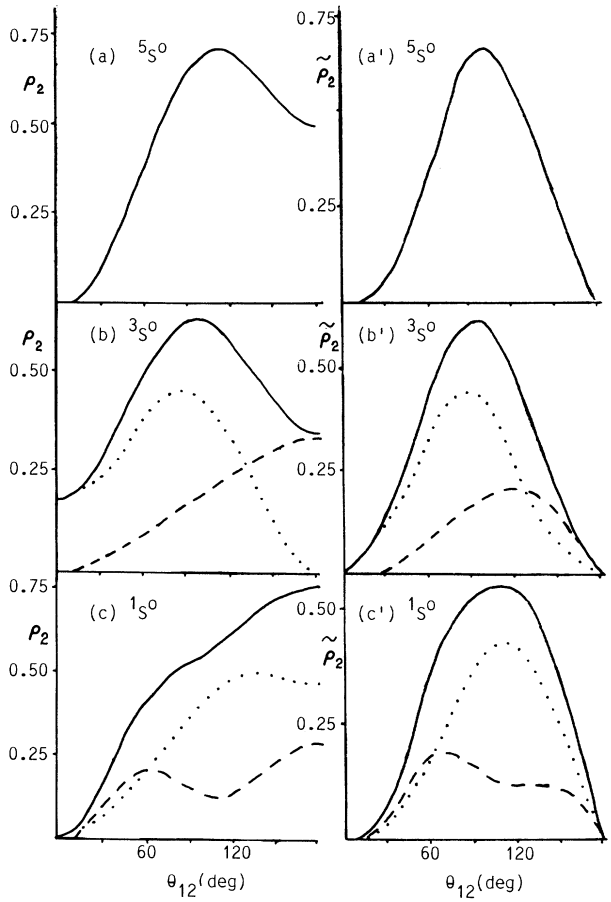

FIG. 2. Spin-dependent and weighted spin-dependent two-body densities as functions of θ_{12}. In the panels on the left-hand side the dashed line is for $\rho_{\frac{1}{2}\frac{1}{2}}+\rho_{\bar{\frac{1}{2}}\bar{\frac{1}{2}}}$ of spin-parallel pairs, the dotted line is for $\rho_{\frac{1}{2}\bar{\frac{1}{2}}}+\rho_{\bar{\frac{1}{2}}\frac{1}{2}}$ of spin-anti pairs, and the solid line is for ρ_2 [in (a), $\rho_2=\rho_{\frac{1}{2}\frac{1}{2}}$]. The panels on the right-hand side are similar but for the weighted densities.

Let us make some suggestions on the motion of the system around the ETH. In the multidimensional coordinate space the minima of the total potential energy $\mathcal{V}=\sum_{(i<j)}V_{ij}$ arise at the ETH's. When the particles leave a minimum, they would like to keep the geometric symmetry as far as they can because in this way $\mathcal{V}$ can be reduced. One possibility is shown in Fig. 4(a), where the motions of particles are correlated such that, say, $\theta_1=180°-\theta_2$, $\phi_1=\phi_2=0$, $\theta_3=\theta_4=90°$, $\phi_3=-\phi_4$, and $\theta_{12}=\theta_{34}$. During this motion an ETH will transform to another ETH via a square. In fact, this possibility is the best choice because $\mathcal{V}$ would be kept in a deep valley during the transformation, as shown by the solid curve in Fig. 5. We call this an ETH-square-ETH (ETH-S-ETH) mode.

Figure 4(a) shows intuitively a classical trajectory. However, the motion along a classical trajectory is not es-

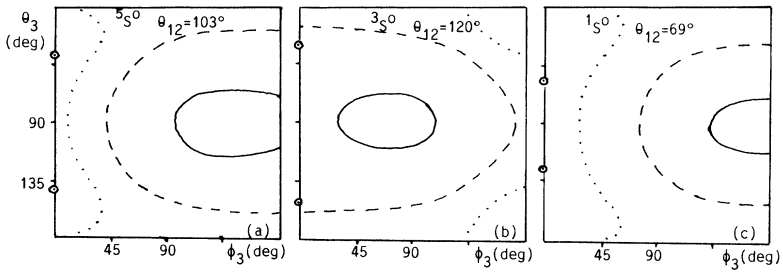

FIG. 3. Spin-dependent three-body densities $\rho_{\frac{1}{2}\frac{1}{2}\mu_3}$ as functions of $\hat{\mathbf{r}}_3$ when the positions of e_1 and e_2 are fixed and marked by two $\odot$ in the figures. The ordinate is for θ_3 form 0° (up) to 180° (down); the abscissa is for ϕ_3. The contours have $\rho_{\frac{1}{2}\frac{1}{2}\mu_3}=\alpha\rho^M$, where ρ^M is the maximum in the figure; $\alpha=25\%$ (outermost, dotted line), 80% (middle, dashed line), and 95% (innermost, solid line), respectively. e_1 and e_2 have their spins up. e_3 and e_4 are both up when M_S is given at 2(a); they are both down when M_S is given at 0 (b) and (c).

tablished in quantum mechanics. Nevertheless, if the wave function is distributed along a classical trajectory, then the motion of the system will have a specific mode associated with this trajectory. In this sense the mode of motion of a quantum state can be defined. Hence, whether the ETH-S-ETH mode exists in the $^5S^o$ state should be subjected to a direct observation of the wave function. On the other hand, the parity and the spatial permutation symmetry may affect the wave function seriously. A striking feature of the odd-parity states is that the coplanar structure (CP), where all four electrons together with the nucleus stay in a plane, is prohibited simply because a reflection of a CP is equivalent to a 180° rotation; thus in this configuration the wave function is equal to zero. Hence, in the above ETH-S-ETH mode, the wave function appears as a node at the square configuration. The reader is reminded that the number of nodes is a measure of vigor of motion. With the above consideration, one would suggest that the $^5S^o$ state may have an energetic ETH-S-ETH motion. This suggestion will be confirmed as follows.

Making use of the preceding findings, let us confine the observation in the subspace of CC and assume the symmetry with respect to the intersection axis. $f_{\frac{1}{2}\frac{1}{2}\frac{1}{2}}$ as a function of θ_1 and ϕ_3 is shown in Fig. 6(a). There is a

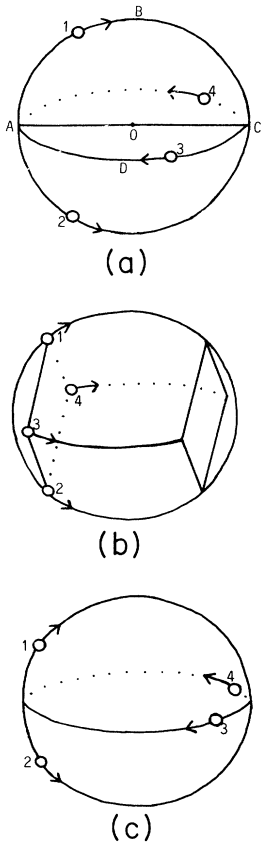

FIG. 4. Intuitive expressions of internal motions. The four electrons are in two pairs and move correlatively. (a) shows the ETH-S-ETH mode where the two pairs move in reverse phase. (b) shows the 4BHC mode where the two pairs move in phase. (c) shows the D2BC mode which is a high-energy version of the ETH-S-ETH mode; in (c) particles 1 and 2 (3 and 4) are much closer to each other than in (a), resulting in energetic collisions.

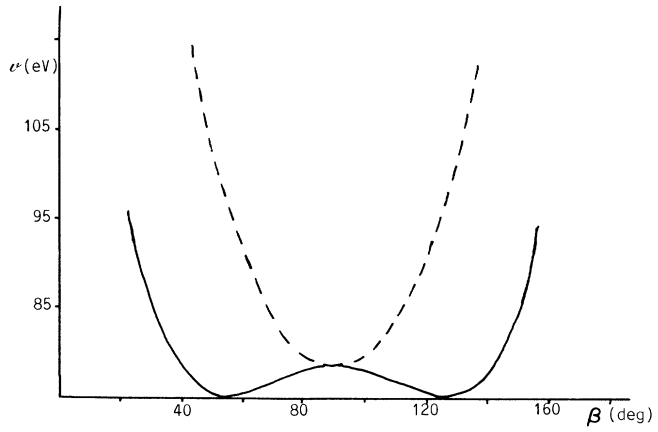

FIG. 5. The solid curve shows the variation of the total potential energy $\mathcal{E}$ during the ETH-S-ETH mode (or D2BC mode); the dashed curve shows that of the 4BHC mode. The electrons are moving in correlation on the conjugate circles shown in Fig. 4. Let β_i be the angle between $\hat{\mathbf{r}}_i$ and the AOC axis (shown in Fig. 4); then in the ETH-S-ETH mode (or D2BC mode) the abscissa $\beta=\beta_1=\beta_2=180-\beta_3=180-\beta_4$; in the 4BHC mode, all β_i are equal to β.

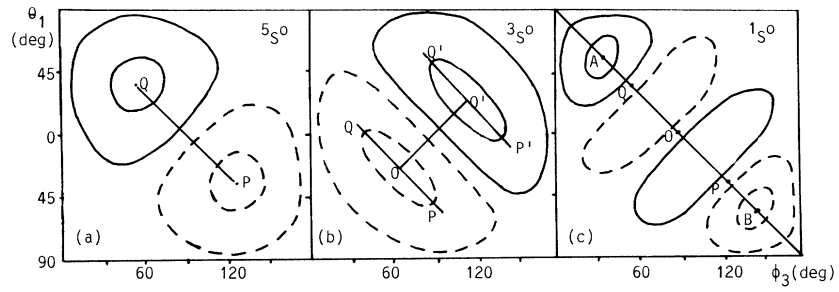

FIG. 6. $\mathrm{Im}f_{\frac{1}{2}\frac{1}{2}\mu_3}$ (the real part is zero) as functions of θ_1 (ordinate) and ϕ_3 (abscissa) while e_1 is confined on the half circle ABC, as shown in Fig. 4 (when e_1 goes from A to C, θ_1 changes as $90°\rightarrow 0°\rightarrow 90°$), and e_3 is confined on the conjugate half circle ADC, e_1 and e_2 (an also e_3 and e_4) keep the symmetry with respect to the AOC axis. e_1 and e_2 always have their spins up; e_3 and e_4 have their spins up in (a) but have their spins down in (b) and (c). When $\mathrm{Im}f_{\frac{1}{2}\frac{1}{2}\mu_3}$ is positive, the contours are shown by solid lines; when $\mathrm{Im}f_{\frac{1}{2}\frac{1}{2}\mu_3}$ is negative, the contours are shown by dashed lines. The outer contour has $\mathrm{Im}f_{\frac{1}{2}\frac{1}{2}\mu_3}=\alpha f^M$ (f^M is the maximum in a figure) with $\alpha=\pm 20\%$, the inner has $\alpha=\pm 84\%$.

peak and a hollow associated with the most probable configurations (the ETH's). These two configurations can transform to each other by crossing the nodal line. An evolution of the system along the line PQ with a node is just the ETH-S-ETH mode. A mode with a node is more important than those without a node (because more energy is concentrated in it). Hence, the ETH-S-ETH mode as an important mode is established.

IV. LOWEST $^3S^o$ STATE

This state has mixed-symmetric [211] spatial permutation symmetry. In principle the frame of reference can be arbitrary chosen; however, we choose the orientation of the frame such that $M_S=0$. It was found that the physical picture is clearer in this choice. Thus we have two spin-up and two spin-down electrons. The geometric structure of this state would be quite different from the $^5S^o$ state, because the ETH is now prohibited. This fact arises because in the ETH configuration the interchange of positions of any pair is equivalent to a reflection together with an appropriate rotation; hence the ETH is only available in odd-parity all-antisymmetric states and in even-parity all-symmetric states.

The $\rho_{\mu_1\mu_2}$ and $\bar{\rho}_{\mu_1\mu_2}$ are shown in Figs. 2(b) and 2(b'). Evidently, the correlation between the spin-parallel pair and that of the spin-anti pair are different. The latter has a bigger chance close to each other. Figure 2(b') shows that the spin-parallel pair prefer to be separated by $\bar{\theta}_{\uparrow\uparrow}=120°$, while the spin-anti pair prefer to be separated by $\bar{\theta}_{\uparrow\downarrow}=87°$. These angular separations suggest that the most probable shape is a square with a diagonal connecting the spin-up pair and another diagonal connecting the spin-down pair, and with the distance between the center of the square and the nucleus $d=r_0/2$. This configuration keeps all the electrons at one side of the nucleus, resulting in higher e-e repulsion. This explains why the energy of this state is higher. Incidentally, in the odd state having two up electrons and two down electrons, any two adjacent vertices of a square (or a rectangle) are not allowed to have spin-parallel electrons. This arises simply because an interchange of the positions of a pair of adjacent spin-parallel electrons together with a simultaneous interchange of the other two is equivalent to a reflection together with a 180° rotation. Hence, the spin-parallel electrons must stay at the two ends of a diagonal.

Let us fix $\phi_1=\phi_2=0°$, $\theta_1=90°-\bar{\theta}_{\uparrow\uparrow}/2$, $\theta_2=90°+\bar{\theta}_{\uparrow\uparrow}/2$ (such that θ_{12} is given at $\bar{\theta}_{\uparrow\uparrow}$), then $\rho_{\frac{1}{2}\frac{1}{2}\frac{1}{2}}$ as a function of $\hat{\mathbf{r}}_3$ is plotted in Fig. 3(b). This figure shows the distribution of a down electron relative to the two up electrons. We found that the pair of down electrons are mainly distributed along $\theta=90°$. When the given θ_{12} is changed, this feature does not change. Hence the $^3S^o$ state prefers the CC just as much as the $^5S^o$ state. However, instead of staying at the opposite sides of the nucleus, the spin-up pair together with the spin-down pair prefer staying at the same side; this is consistent with the analysis from Fig. 2(b').

Let us make some suggestions on motions around the square. Since in the most probable shape the electrons are concentrated at one side of the nucleus, the Coulomb repulsion will push the electrons and make the square "breathe" as shown in Fig. 4(b). In this way the geometric symmetry is kept, and the small square transforms to a large square, and again to a small square at the opposite side. Since the contraction of a square implies a four-body head-on collision, we shall call the breathing in a sphere a 4BHC mode. In this mode successive four-body collisions occur at the two sides of the nucleus in turns.

Since this state prefers also the CC structure let us confine the observation in the same subspace of Fig. 6(a); then $f_{\frac{1}{2}\frac{1}{2}\frac{1}{2}}$ as a function of θ_1 and ϕ_3 is shown in Fig. 6(b). There is a peak 0' and a hollow 0 related to the two squares at the two sides of the nucleus. Evidently, the evolution from 0 to 0', forth and back, is the main mode because a node (arising at the CP structure) is involved. It is just the 4BHC mode. However, the wave function is

also distributed smoothly along the lines PQ and $P'Q'$, which implies the possibility of deviating from the square shape. If the electrons that move in the CC are exactly in phase (the angles between all $\hat{\mathbf{r}}_i$ and the intersection axis are the same), the square shape is exactly kept. However, if two on a circle arrive at the left- (or right-) hand side later than the other two on the other circle, there would be a delay in phase; accordingly the diffusion along PQ and $P'Q'$ appears. Hence this state is dominated by the 4BHC mode. However, there is a remarkable diffusion in phase. It is noticed that in the investigation of the three-electron intrashell states [9,10], a similar mechanism, namely, the three-body head-on collision (3BHC), was found both in the $^4S^o$ and $^2S^o$ odd-parity states. Undoubtedly, this is a basic mechanism existing in atomic systems. The 4BHC mode is a very energetic mode because ω varies rapidly during the motion. This is shown by the dashed curve in Fig. 5, where the steepness of the curve is impressive.

Incidentally, if we make the choice $M_S=1$, the preference of the CC structure remains. Now we have three up electrons and one down electron. The up-down pair staying in one of the circles is found not to keep the symmetry with respect to the intersection axis. Consequently, a clear picture of internal motions cannot be obtained.

V. LOWEST $^1S^o$ STATE

This state has mixed-symmetric [22] spatial permutation symmetry. Since M_S has to be zero, there are two up electrons and two down electrons.

The $\rho_{\mu_1\mu_2}$ and $\tilde{\rho}_{\mu_1\mu_2}$ are shown in Figs. 2(c) and 2(c'). These figures are very different from 2(b) and 2(b') because the $\tilde{\rho}_{\frac{1}{2}\frac{1}{2}}+\tilde{\rho}_{\frac{1}{2}\frac{1}{2}}$ is peaked at the left-hand side with $\bar{\theta}_{\uparrow\uparrow}=69°$. It implies that now the two spin-parallel electrons prefer to be close to each other.

Let $\phi_1=\phi_2=0°$, $\theta_1=90°-\bar{\theta}_{\uparrow\uparrow}/2$, $\theta_2=90°+\bar{\theta}_{\uparrow\uparrow}/2$; then $\rho_{\frac{1}{2}\frac{1}{2}\frac{1}{2}}$ as a function of $\hat{\mathbf{r}}_3$ is plotted in Fig. 3(c). This figure also shows the distribution of a down electron relative to the two up electrons. Just as in Figs. 3(a) and 3(b), the system prefers the CC structure; however, Fig. 3(c) is closer to 3(a) but quite different from 3(b) because the spin-up pair and the spin-down pair are separated at opposite sides of the nucleus.

In order to inspect the correlated motions in the CC, we confine the observation in the same subspace as Fig. 6(a); then $f_{\frac{1}{2}\frac{1}{2}\frac{1}{2}}$ as a function of θ_1 and ϕ_3 is shown in Fig. 6(c). This figure reveals a very strong oscillation associated with the trajectory AB connecting the maximum A and the minimum B. In fact, this is the same trajectory as in Fig. 6(a) but it has two more nodes. The nodes P and Q appear at the ETH shape. This shape is prohibited due to the reason stated in the first paragraph of Sec. IV. The node O appears at a CP structure. This structure is prohibited in all odd-parity $L=0$ states. These three nodes imply a very vigorous oscillation with a large amplitude; this explains why this state is much higher in energy. During this oscillation two-body collisions occur simultaneously at the opposite sides of the nucleus, as shown intuitively in Fig. 4(c), where 1 and 2, and simultaneously 3 and 4, have just undergone collisions. After the collisions, all four electrons move back along the CC to undergo the successive two-body collisions. This mode is a high-energy version of the ETH-S-ETH mode, and is called a double two-body collisions (D2BC) mode. In the D2BC mode, the ETH is no longer the most probable shape but associated only with a node in the oscillation. Instead, now the most probable shape [associated with the maximum A and minimum B in Fig. 6(c)] is a prolonged ETH (PETH) stretching along the intersection axis of the CC, as shown in Fig. 4(c). A pair of spin-parallel electrons is at the one end of the PETH while the other pair is at opposite end. Incidentally, the diffusion in phase is also observed in this mode.

VI. FINAL REMARKS

(i) There are two parameters in our model, r_0 and $l_{\max}$. Let us examine how these parameters affect the results. In the case of $^5S^o$ states, if we change r_0 from 0.62 Å to 0.7 Å (but keep $l_{\max}=2$), there is a great change in energies; E_i (in eV, $i=1-3$) are changed from 160.56, 256.03, and 314.26 to 136.09, 213.26, and 258.34, respectively. However, the change in wave functions is very small. The overlaps of the two wave function (the angular part) with different r_0,

$$\langle \Psi_i(r_0=0.7, l_{\max}=2) | \Psi_i(r_0=0.62, l_{\max}=2) \rangle \ , \tag{11}$$

are equal to 0.9997, 0.9991, and 0.9995 for $i=1$, 2, and 3, respectively. The great overlap appears not only in the $^5S^o$ states but also in other $^{2S+1}S^o$ states. Hence, the above results on angular motion do not depend on r_o in the qualitative sense.

In the $^5S^o$ states if we change $l_{\max}$ from 2 to 3 (but keep $r_0=0.62$ Å), the energies of the three lowest states are changed to 160.31, 253,83, and 310.89 eV. The change is small, particularly in the lowest state. The overlaps

$$\langle \Psi_i(r_0=0.62, l_{\max}=2) | \Psi_i(r_0=0.62, l_{\max}=3) \rangle \tag{12}$$

are equal to 0.9991, 0.9844, and 0.9485 for $i=1$, 2, and 3, respectively. If we change $l_{\max}$ from 2 to 1 (but keep $r_0=0.62$ Å), the energy is changed to 161.67 eV (instead of three, now there is only one state). The overlap

$$\langle \Psi_1(r_0=0.62\ ,\ l_{\max}=2) | \Psi_1(r_0=0.62\ ,\ l_{\max}=1) \rangle \tag{13}$$

is equal to 0.9942. Evidently, the effect of $l_{\max}$ is explicit. However, if only the lowest state is concerned, the change is quite small. This holds also for other $^{2S+1}S^o$ states. Hence, the above results on angular motion of the lowest states are not sensitive to $l_{\max}$.

Since our model is insensitive to inherent parameters, if only the lowest $^{2S+1}S^o$ state are concerned, the qualitative findings of this paper are general to angular motion. It was stated that the intrashell states are characterized by the angular motion and not by the radial motion. Hence, the above findings are expected to provide a qualitative description of the lowest intrashell states. In fact, a work on $^1S^e$ states of four-electron atoms [12] supports

this suggestion. However, all of the above findings have to be checked in the future by direct realistic calculation.

(ii) There are two essential factors in determining the structure: one is the geometric symmetry; the other is the quantum-mechanic symmetry (e.g., the parity, the spatial permutation symmetry with respect to the interchange of positions). The system prefers having better geometric symmetry as far as possible; because in this way the total potential energy $\mathcal{V}$ can be reduced, and periodic motion may be preserved (as shown below). On the other hand, there are nodal surfaces arising from quantum-mechanic symmetry appearing in the multidimensional coordinate space. They can be called inherent nodal surfaces because they have to appear at the exact locations for all the states of a given $^{2S+1}L^{\pi}$ symmetry. These inherent surfaces strongly affect the structures; because they impose strict restrictions on the choice of the most probable shape (in order to reduce kinetic energy the most probable shape would not be close to these surfaces) and because they direct the system to undergo a specific mode of motion by evolving across these surfaces.

For example, the ETH has the best geometric symmetry, and it turns out to be the most probable shape of the $^5S^o$ state. However, this favorable shape is prohibited in the $^3S^o$ and $^1S^o$ states, resulting in higher energies. Instead, the $^3S^o$ state chooses the square, and the $^1S^o$ state chooses the PETH. One more example is the CP structure which is prohibited in all odd-parity $L=0$ states; it associates with an inherent nodal surface. It turns out that all modes found in this paper are related to this surface by crossing it.

(iii) Although it is clear that the odd-parity states having different spatial permutation symmetries have different structures, they have a common feature: they all prefer the CC configuration. This is a striking feature. In CC, the two electrons on a circle have their spins parallel to each other, and when they move they keep the symmetry with respect to the intersection axis. While they move forth and back along the circles, two-body collisions occur. There are two cases. In the first case the two-body collisions occur simultaneously in one side of the nucleus, such that these two collisions constitute a four-body head-on collision, i.e., the 4BHC mode of the $^3S^o$ state shown in Fig. 4(b). In the second case the two-body collisions occur in opposite sides, i.e., the D2BC mode of the $^1S^o$ state shown in Fig. 4(c) (the ETH-S-ETH mode of the $^5S^o$ state is a low-energy version of this mode). In the first case, the four electrons are kept at the same side of the nucleus; in the second case, two pairs of electrons are mostly kept at opposite sides. Recall that in the doubly excited helium states, a quantum number K was introduced to specify the angular correlation [13–15]. Since strong angular correlation has also been found in the states of four-electron atoms, this correlation results also in remarkable geometric character; thus a quantum number similar to K can be introduced to classify the quadruply excited states.

(iv) We have investigated only the $L=0$ states where the spatial part of the wave function is isotropic. However, if $L\neq 0$, it will be interesting to see how serious is the effect of the collective rotation on the modes of internal motion and how the intersection axis of the CC chooses its direction relative to **L**. Another quantum number similar to I of doubly excited states may be introduced to specify the relative orientation of **L** and the intersection axis.

(v) We have used a spin-dependent procedure in analyzing particle correlations. This is necessary; otherwise we would have an ambiguous picture. Figure 2 shows clearly that the correlation of the two spin-parallel particles and that of the two spin-anti particles are completely different. In fact, the up electron and the down electron play different roles in constituting the structure. For example, it is the spin-parallel electrons staying at one end of the PETH. Similarly, in Sec. IV, each diagonal of the square has two spin-parallel (but cannot be spin-anti) electrons at its two ends.

(vi) It was mentioned that both the all-symmetric S^e states and the all-antisymmetric S^o states are allowed to have the ETH structure. In our model, if we keep the dynamics but change the parity and the spatial permutation symmetry, then the lowest all-symmetric S^e state has a much lower energy (122.85 eV), and has the most probable shape, an ETH, as it should be. One may ask why the two similar geometric structures of the odd and even states differ greatly in energy. This arises because in the even-parity case the inherent nodal surface at the CP configuration disappears, resulting in a much more stable structure. This example shows how the inherent surface affects the motion and increases the kinetic energy. Though the all-symmetric S^e symmetry is not realistic in four-electron systems it is very important in four-valence-nucleon systems.

(vii) It is notable that the two basic modes found in this paper, namely, the 4BHC and D2BC modes, are closely related to periodic solutions of classical mechanics. When four electrons are confined on a sphere with radius r_0, the classical set of eight Lagrange's equations read

$$mr_0^2\ddot{\theta}_i = mr_0^2\dot{\phi}_i^2\sin\theta_i\cos\theta_i - \frac{e^2}{2\sqrt{2}r_0}\sum_{j(\neq i)}(\cos\theta_i\cos\phi_i\sin\theta_j\cos\phi_j+\cos\theta_i\sin\phi_i\sin\theta_j\sin\phi_j-\sin\theta_i\cos\theta_j)(1-\cos\theta_{ij})^{-3/2}\ ,$$

$$mr_0^2[(\sin^2\theta_i)(\ddot{\phi}_i)+(\sin 2\theta_i)(\dot{\theta}_i\dot{\phi}_i)] = -\frac{e^2}{2\sqrt{2}r_0}\sum_{j(\neq i)}(-\sin\theta_i\sin\phi_i\sin\theta_j\cos\phi_j+\sin\theta_i\cos\phi_i\sin\theta_j\sin\phi_j)(1-\cos\theta_{ij})^{-3/2}\ ,$$

(14)

where i is from 1 to 4. Though the general solution is difficult to obtain, it turns out that the solution

$$\phi_1=0^\circ\ ,\quad \phi_2=90^\circ\ ,\quad \phi_3=180^\circ\ ,\quad \phi_4=270^\circ\ ;$$
$$\theta_1=\theta_2=\theta_3=\theta_4=\theta(t)\ , \tag{15}$$

with $\theta(t)$ satisfying

$$\beta\ddot{\theta}=\frac{\cos\theta}{\sin^2\theta}\ ,\quad \beta=\frac{4mr_0^3}{(2\sqrt{2}+1)e^2}\ , \tag{16}$$

is an exact solution of Eq. (14). In fact, Eq. (16) belongs to the same type of equation that we have found in the 3BHC mode of three-electron atomic systems [9]. Equation (16) can be integrated; then we have

$$\dot{\theta}^2=\frac{2}{\beta}\left[\frac{1}{\sin\theta_0}-\frac{1}{\sin\theta}\right]\ . \tag{17}$$

It implies a periodic collective oscillation back and forth between θ_0 and $180^\circ-\theta_0$. The period of oscillation is

$$\mathcal{T}=\sqrt{2\beta}\int_{\theta_0}^{180^\circ-\theta_0}\left[\frac{1}{\sin\theta_0}-\frac{1}{\sin\theta}\right]^{-1/2}d\theta\ . \tag{18}$$

Evidently, this periodic solution is just the 4BHC mode shown in Fig. 4(b).

Furthermore, it turns out that the next solution

$$\phi_1=0^\circ\ ,\quad \phi_2=90^\circ\ ,\quad \phi_3=180^\circ\ ,\quad \phi_4=270^\circ\ ;$$
$$\theta_1=180^\circ-\theta_2=\theta_3=180^\circ-\theta_4=\theta(t)\ , \tag{19}$$

with $\theta(t)$ satisfying

$$\gamma\ddot{\theta}=\cos\theta\sin\theta\left[\frac{1}{(1-\cos2\theta)^{3/2}}-\frac{1}{(1+\cos^2\theta)^{3/2}}\right]\ ,\quad \gamma=\frac{\sqrt{2}mr_0^3}{e^2}\ , \tag{20}$$

is also an exact solution of Eq. (14). Equation (20) can be integrated; then we have

$$\dot{\theta}^2=\frac{1}{\gamma}\left[\frac{1}{\sqrt{2}}\left[\frac{1}{\sin\theta_0}-\frac{1}{\sin\theta}\right]+2\left[\frac{1}{(1+\cos^2\theta_0)^{1/2}}-\frac{1}{(1+\cos^2\theta)^{1/2}}\right]\right]\ . \tag{21}$$

It also implies a periodic collective oscillation back and forth between θ_0 and $180^\circ-\theta_0$. The period of oscillation now is

$$\mathcal{T}=2\sqrt{\gamma}\int_{\theta_0}^{180^\circ-\theta_0}\left[\frac{1}{\sqrt{2}}\left[\frac{1}{\sin\theta_0}-\frac{1}{\sin\theta}\right]+2\left[\frac{1}{(1+\cos^2\theta_0)^{1/2}}-\frac{1}{(1+\cos^2\theta)^{1/2}}\right]\right]^{-1/2}d\theta\ . \tag{22}$$

Evidently, this periodic solution is just the D2BC mode shown in Fig. 4(c). Now it is clear that the basic modes of motion in quantum states correspond to periodic solutions of classical mechanics.

APPENDIX

The following two formulas are used to obtain analytical expressions of two- and three-body densities for carrying out the numerical calculation.

(1) Let $(Y_{l_a}(\hat{\mathbf{r}}_1)Y_{l_b}(\hat{\mathbf{r}}_2))_l$ be denoted as $(l_a(1)l_b(2))_l$. Let $\sqrt{2l+1}$ be denoted as $\hat{l}$. Then the first formula is as follows:

$$d\hat{\mathbf{r}}_3 d\hat{\mathbf{r}}_4[(l_a'(1)l_b'(2))_{l_1'}(l_c'(3)l_d'(4))_{l_2'}]^*_{\mathcal{L},\mathcal{M}}[(l_a(1)l_b(2))_{l_1}(l_c(3)l_d(4))_{l_2}]_{\mathcal{L}\mathcal{M}}$$
$$=\delta_{l_c l_c'}\delta_{l_d l_d'}\delta_{l_2 l_2'}(-1)^{\mathcal{L}+l_2+l_1'}\hat{\mathcal{L}}\sum_{\lambda}\hat{\lambda}W(l_1l_1'\mathcal{L}\mathcal{L}\ ,\ \lambda l_2)C^{\mathcal{L}\mathcal{M}}_{\lambda,0\,\mathcal{L}\mathcal{M}}$$
$$\times\sum_{\lambda_a,\lambda_b}\hat{l}_1\hat{l}_1'\hat{\lambda}_a\hat{\lambda}_b U\begin{bmatrix} l_a & l_b & l_1\\ l_a' & l_b' & l_1'\\ \lambda_a & \lambda_b & \lambda\end{bmatrix}\frac{\hat{l}_a'\hat{l}_b'}{4\pi}C^{l_a\,0}_{\lambda_a 0\,l_a' 0}C^{l_b\,0}_{\lambda_b 0\,l_b' 0}(Y_{\lambda_a}(\hat{\mathbf{r}}_1)Y_{\lambda_b}(\hat{\mathbf{r}}_2))_{\lambda 0}\ . \tag{A1}$$

(2) The second formula is as follows:

$$\int d\hat{\mathbf{r}}_4[(l_a'(1)l_b'(2))_{l_1'}(l_c'(3)l_d'(4))_{l_2'}]^*_{\mathcal{LM}}[(l_a(1)l_b(2))_{l_1}(l_c(3)l_d(4))_{l_2}]_{\mathcal{LM}}$$

$$=\delta_{l_a l_d'}(-1)^{l_a+l_b+l_c+l_d+\mathcal{L}}\hat{l}_1\hat{l}_1'\hat{l}_2\hat{l}_2'\hat{l}_a\hat{l}_a'\hat{l}_b\hat{l}_b'\hat{l}_c\hat{l}_c'(4\pi)^{-3/2}$$

$$\times\hat{\mathcal{L}}\sum_{\lambda,\lambda'}(-1)^{\lambda'}(2\lambda+1)(2\lambda'+1)\left[\sum_{\lambda_0}\hat{\lambda}_0 W(\lambda\lambda'\mathcal{L}\mathcal{L},\lambda_0 l_d)C^{\mathcal{LM}}_{\lambda_0 0\,\mathcal{LM}}\right.$$

$$\times\sum_{k_1,k_c}\hat{\mathbf{k}}_1 U\begin{bmatrix} l_1 & l_c & \lambda \\ l_1' & l_c' & \lambda' \\ k_1 & k_c & \lambda_0 \end{bmatrix}\sum_{k_a,k_b} U\begin{bmatrix} l_a & l_b & l_1 \\ l_a' & l_b' & l_1' \\ k_a & k_b & k_1 \end{bmatrix}C^{k_a\,0}_{l_a 0\,l_a' 0}C^{k_b\,0}_{l_b 0\,l_b' 0}C^{k_c\,0}_{l_c 0\,l_c' 0}$$

$$\left.\times[(Y_{k_a}(\hat{\mathbf{r}}_1)Y_{k_b}(\hat{\mathbf{r}}_2))_{k_1}Y_{k_c}(\hat{\mathbf{r}}_3)]_{\lambda_0 0}\right]$$

$$\times W(l_1 l_c\mathcal{L}l_d;\lambda l_2)W(l_1'l_c'\mathcal{L}l_d';\lambda' l_2')\ . \tag{A2}$$

In the case of $\mathcal{L}=0$, these two formulas can be considerably simplified.

[1] C. G. Bao, T. K. Lim, and W. Q. Chao, Nucl. Phys. **A439**, 456 (1985).

[2] Y. Komninos and C. A. Nicolaides, J. Phys. B **19**, 1701 (1986); C. A. Nicolaides and Y. Komninos, Phys. Rev. A **35**, 999 (1987).

[3] Y. Komninos, M. Chrysos, and C. A. Nicolaides, J. Phys. B **20**, L791 (1987).

[4] C. A. Nicolaides, M. Chrysos, and Y. Komninos, J. Phys. B **21**, L73 (1988).

[5] Y. Komninos, M. Chrysos, and C. A. Nicolaides, Phys. Rev. A **38**, 3182 (1988).

[6] C. A. Nicolaides, M. Chrysos, and Y. Komninos, Phys. Rev. A **41**, 5244 (1990).

[7] S.Watanabe and C. D. Lin, Phys. Rev. A **36**, 511 (1987).

[8] C. G. Bao, Z. Phys. D **22**, 557 (1992).

[9] C. G. Bao, J. Phys. B **25**, 3725 (1992).

[10] C. G. Bao, Few-Body Sys. **13**, 41 (1992).

[11] M. Karplus and R. N. Porter, *Atoms and Molecules* (Benjamin, New York, 1970).

[12] C. G. Bao, J. Phys. B **25**, 3245 (1992).

[13] D. R. Herrick and O. Sinanoglu, Phys. Rev. A **11**, 97 (1975).

[14] C. D. Lin, Adv. At. Mol. Phys. **22**, 77 (1986).

[15] C. G. Bao and Y. W. Duan, Phys. Rev. A **46**, 125 (1992).